AIMS Materials Science, 3(3): 1160-1176.
DOI: 10.3934/matersci.2016.3.1160
Received: 11 May 2016
Accepted: 03 August 2016
Published: 11 August 2016

http://www.aimspress.com/journal/Materials

Research article

Co-Sintering behaviour of zirconia-ferritic steel composites

Tim Slawik, Anne Günther, Tassilo Moritz *, and Alexander Michaelis

Fraunhofer IKTS, Winterbergstraße 28, 01277 Dresden, Germany

*** Correspondence:** Email: tassilo.moritz@ikts.fraunhofer.de.

Abstract: The combination of metallic and ceramic materials allows the combination of positive properties of both and can be applied in various industrial fields. At the moment, the deployment of these composites faces difficult and complex manufacturing. One attempt, which offers a short process route and a high degree of flexibility regarding design is a combined shaping (co-shaping) with a combined sintering (co-sintering). The article will show co-sintering results of different metal-ceramic symmetric and asymmetric multi-layered tapes, consisting of yttria stabilized zirconia combined with a ferritic iron chromium steel. Focus is on the densification and co-sintering behaviour of ceramic layers depending on the sintering behaviour of metallic layers. Co-sintered composites were characterized by field emission scanning electron microscopy, x-ray diffraction measurements and in terms of adhesive tensile strength.

Keywords: metal-ceramic composite; co-sintering; porous-dense combination; tensile strength

1. Introduction

The development of new materials is often the beginning of innovative and future-oriented technologies. This is necessary to meet tomorrow's engineering applications, for example, to increase efficiency, reliability and productivity or to reduce energy consumption and with this to raise standard of living [1,2].

It is also possible to understand the term "*new material"* as a combination of materials. Joining metals and ceramics for example, allows the combination of the positive properties of both. Metallic materials offer magnetic properties, a high ductility or an electrical conductivity, while ceramic materials have a high strength even at elevated temperatures, a high corrosion resistance and, in the case of zirconia, an oxygen-ion conductivity.

These combinations are necessary in solid oxide fuel cells, gas separation membranes, thermoelectric generators, bipolar surgical tools or in mechanical engineering applications. Major obstacle for using these composites is, that existing manufacturing technologies cannot fulfil requirements in terms of costs, complex geometries or operation conditions.

Conventional frictional and form-locking joining techniques, like screwing or shrinking, offer a simple possibility to combine both materials. However, these joining techniques have many disadvantages regarding wall thicknesses and geometrical design.

Conventional cohesive joining techniques, like gluing or brazing, allow chemical bonding between both materials. Especially gluing allows a simple joining, while for brazing a special development of brazing material is necessary [3]. However, within both processes a further material is inserted which can limit functionality, operation temperature or strength. Nevertheless, brazing is already well established for joining power electronics or stacks of solid oxide fuel cells.

It is generally known that in addition to conventional joining techniques several powder technological approaches exist. One of these approaches is thermal spraying. This is used for applying a metallic or ceramic layer on top of ceramic or metallic substrate [4]. This allows the production of electrical circuits on insulating substrates, wear-resistant layers or thermal barrier coatings. Layer thicknesses thereby range from 30 µm to some millimetres. The high layer thickness is a disadvantage as well as the high porosity and high surface roughness. Furthermore, the coating of complex geometries is quite difficult.

One promising approach to simplify the production of composites and achieving a high degree of freedom regarding design is a co-shaping, continued with co-sintering. Especially the co-sintering step is the challenge of this manufacturing route. Differences in coefficient of thermal expansion (CTE) or in densifying behaviour (shrinkage) can lead to stresses during heating or cooling [5]. These stresses can cause flaws as cracks, delaminations, pores, changes in microstructure or in the case of asymmetric composites a warpage. Cai et al. has theoretically analysed occurring stresses during sintering of composites [5]. He considered that the materials exhibit during sintering pure viscous behaviour and developed, based on this assumption, equations for maximum stresses σ_K in bi-layered asymmetric (equation 1) and three-layered symmetric (equation 2) composites.

$$\sigma_K = \left[\frac{m^4+m\,n}{n^2+2\,m\,n\,(2\,m^2+3\,m+2+\,m^4\,)}\right]\eta\,\Delta\dot{\varepsilon} \tag{1}$$

$$\sigma_K = \frac{1}{1+m\,n}\,\eta\,\Delta\dot{\varepsilon} \tag{2}$$

Especially his equation for the rate of warping (equation 3), which was derived from equation 1, is commonly used for a comparison of theory and practice [6,7,8].

$$\dot{k} = \frac{6\,(m+1)^2\,m\,n}{m^4\,n^2+2\,m\,n\,(2m^2+3\,m+2)+1}\,\Delta\dot{\varepsilon} \tag{3}$$

It can be derived from these equations that besides of the difference in CTE and sintering behaviour, which is represented as difference in sintering strain rate $\Delta\dot{\varepsilon}$, the ratio of layer thickness m and the material viscosity η respectively ratio of the material viscosities n influence stresses and warpage.

Furthermore, it is known that non- or low-shrinking substrates can harm and slow down densifying of thin ceramic layers during co-sintering, which result in lower densities in comparison to free shrinking materials [9,10,11]. In this context Yamaguchi et al. and Muecke et al. showed that high densities in co-sintered ceramic layers can only be reached, if differences in strain rate are small enough or if the negative effect is compensated by an increased isothermal dwell time [11,12].

The first step to avoid flaws during co-sintering is the choice of materials with well adapted CTE's. The second step is the reduction of mismatches in sintering strain rate. The main focus of investigations for the second step is the adaptation of green densities, use of specific particle sizes, changing heating rates, using doping elements or integrating a material gradient [13–17]. In this work, sintering behaviour was influenced and adjusted by treating metallic powder with a high energy milling step [18,19].

The aim of this work was to achieve a multi-layered composite consisting of a thin ceramic layer on top or between two thicker porous metallic layers. These composites are suitable as semi-finished metal supported fuel cells, filter elements or gas separation membranes. Thereby, investigations about the co-sintering behaviour of adapted and un-adapted composites were done. A combination of zirconia and stainless steel as materials was used. The composites were produced by using a tape casting process, which is the standard process in ceramic industry for the production of large-area, thin and flat ceramic substrates [20].

2. Materials and Method

For the investigations 3 mol% yttrium stabilized zirconia TZ-3YS-E (Tosoh Inc., Japan) was selected as ceramic material and the gas atomized high temperature corrosion resistant ferritic iron-chromium alloy Crofer®22APU (H. C. Starck GmbH, Germany) as metallic one. The metallic powder was treated with a high energy milling step, to influence its sintering behaviour. Further information about this can be found in earlier publications [18,19,21]. Overall, four different metallic powders (metal powder 1–4) were taken, which differentiate in terms of their sintering behaviour. Crofer®22APU was chosen due to its melting temperature of 1510 °C which is above the sintering temperature of 1450 °C of the zirconia powder.

Different metal-ceramic (asymmetric) and metal-ceramic-metal (symmetric) composites were produced by tape casting. For this a slurry consisting of water, polyvinylalcohol as binder and glycerine as plasticizer was prepared. Polyvinylalcohol and glycerine were taken due to their good decomposition behaviour under hydrogen atmosphere, which is important to avoid a harmful increase of carbon content in steel after sintering [22]. Besides binder and plasticizer, the defoamer Foammaster F111 (BASF SE, Germany) and the surfactant Glycol N 109 (Zschimmer & Schwarz GmbH % Co. KG, Germany) were used. The composition of the individual slurries is shown in table 1. More details concerning the production process are published in [18,22,23].

Tape casting allows the production of asymmetric and symmetric composites. Asymmetric composites were produced with the combination TZ-3Y-SE and metal powder 1 (composite 1a) respectively powder 2 (composite 2). Symmetric composites were produced with metal powder 3 (composite 3), powder 4 (composite 4) and again with powder 1 (composite 1s). The ceramic green layer thickness was in all cases 11.6 ± 1 µm while the metallic layer thickness varied from 200 to 400 µm. Hence, the metallic layer thickness is 17 to 34 times thicker than the ceramic one. It has to be noted that the specific metallic layer thickness has no influence on the shown results, for which

reason it is not specified in detail. Figure 1 exhibits an asymmetric metal-ceramic multi-layered green tape out of composite 2. The ceramic layer thickness was measured before and after sintering using field emission electron scanning microscopy (FESEM) (NVision 40, Carl Zeiss SMT GmbH, Germany).

Table 1. Composition of ceramic and metallic slurries for tape casting in wt%.

	powder	water	binder	plasticizer	de-foamer	surfactant
TZ-3YS-E	44.5	45.1	4.3	5.7	0.2	0.2
metal powder 1	43.3	35.7	4.3	6.5	0.1	0.1
metal powder 2	80.5	15.6	1.6	2	0.1	0.2
metal powder 3	65.3	28.1	3	3.3	0.1	0.2
metal powder 4	80.5	15.6	1.6	2	0.1	0.2

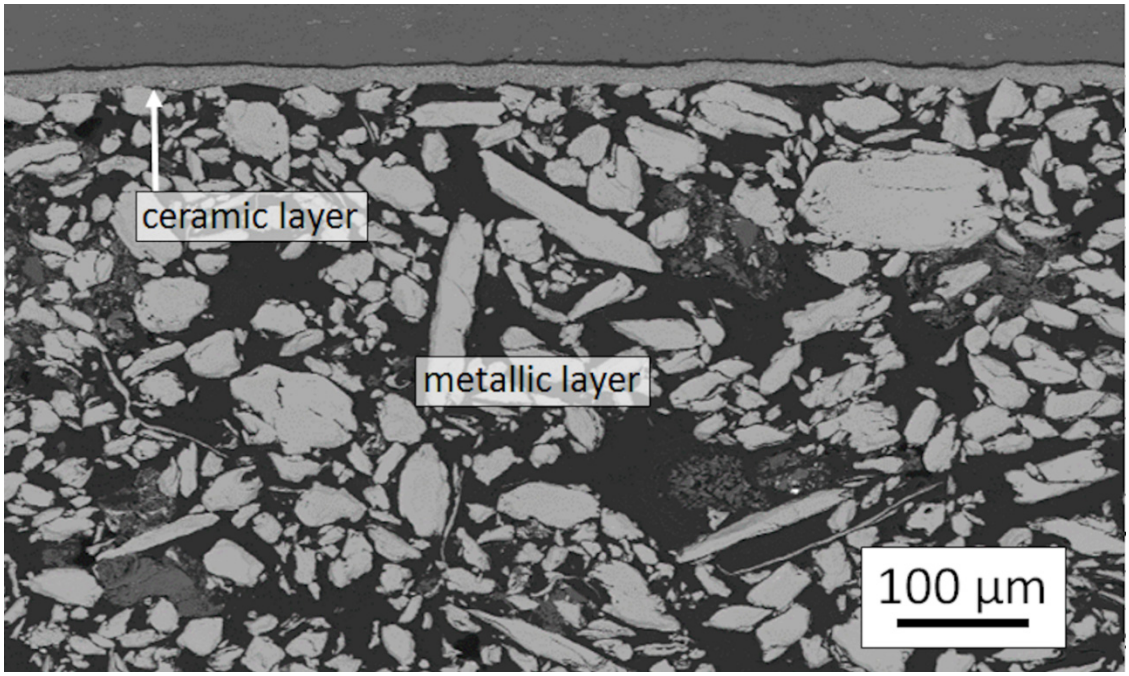

Figure 1. Metal-ceramic asymmetric green tape with the thin ceramic on top of the thicker metallic layer.

Round specimens with a diameter of 20 mm were punched out of the tapes for co-sintering experiments. These tapes were debinded and sintered on top and between two porous, 1 mm thick Keralpor 99 alumina sintering supports (Kerafol Keramische Folien GmbH, Germany) respectively. Covering the tapes with a sintering support was necessary to avoid warpage during sintering. Furthermore, two smaller specimens with a rectangular shape and dimensions of 5 × 7 mm out of composite 1a and 2 were sintered without a coverage.

The specimens were debinded under hydrogen atmosphere with a heating rate of 1 K/min up to 600 °C. After a dwell time of 2 h the furnace (RRO280/300-900V, MUT advanced heating, Germany) was cooled down to room temperature with a rate of 3 K/min. Sintering took place in a separated

furnace (HTBL20W22-2G, Carbolite Gero GmbH & Co. KG, Germany) with a heating rate of 3 K/min up to the sintering temperature between 1200 and 1400 °C and a cooling rate of 4 K/min. The dwell time was 2 h and the sintering atmosphere was a mixture of argon (80%) and hydrogen (20%).

The sintering behaviour of the materials was characterized with high temperature heating microscope (EHM 201-17K, Hesse Instruments, Germany). Thereby a camera records pictures of the specimen during sintering in a tube furnace. A following image analyses allows a calculation of linear shrinkage as well as sintering strain rate. During this measurement the tube furnace was flushed with gas (95% argon, 5% hydrogen). Heating rate was 1 K/min up to 600 °C and then 3 K/min up to 1400 °C. The used specimens were 1 mm in thickness and had a diameter of 5 mm. Using a heating microscope instead of pushing rod dilatometer, had the advantage to get free shrinkage curves of the materials. When using a pushing rod dilatometer, the pressure of the pushing rod can especially falsify the measurement of the metallic material due to its low viscosity at high temperatures.

The pushing rod dilatometer Dil 402 D (Netsch Gerätebau GmbH, Germany) was used for measuring the CTEs. The CTE was measured by means of sintered laminates (density > 99%) of each material with dimensions of 4 × 4 × 20 mm^3.

The sintered composites were cut in the middle and were prepared by grinding and polishing with abrasive papers for microstructural investigations with the field emission scanning microscope NVision 40 (Carl Zeiss SMT GmbH, Germany),. The green tapes, however, were prepared using broad ion beam method. 10–15 pictures with a magnification of 7000 and a backscattered electron detector, which shows the material contrast, were taken to analyse porosity. The porosity was afterwards determined by image analysing with the software ImageJ V1.6.0 (National Institute of Health, USA).

The viscosity of the ceramic and metallic materials during sintering was measured using the bending beam method. This method is usually used to measure the viscosity of glasses [24] but was adapted by Lee et al. [25] and Lame et al. [26] to measure the viscosity of oxide ceramics and steels during sintering. Thereby, a beam is sintered on top of a special support which has only two contact points at the left and right side of the tape. It is then possible to calculate the viscosity η from the rate of deflection $\dot{\delta}$ using equation 4 [27].

$$\eta = \frac{5\,\rho\,g\,L^4}{32\,\dot{\delta}\,h^2} \tag{4}$$

The span length L during the measurements amounted 10 mm. After preliminary tests, the thickness h of the tapes was set to 100 µm for the ceramic and 500 µm for the metallic. These tapes were pre-sintered up to 1000 °C to avoid a bending during de-binding and to give the tapes some strength.

Before and after co-sintering, the ceramic layer of the asymmetric composites was investigated in terms of its phase composition by using x-ray diffraction (Bruker D8 ID 3003TT, Bruker Corporation, USA).

The tensile adhesive strength between the ceramic and metallic layers was measured using the symmetric structured composite 1s and, furthermore, composites with dense metallic layers. The powder treatment and the composition for the dense sintering metallic tapes is published in [19]. For testing round specimens with a diameter of approximately 25 mm (after sintering) were prepared and sintered at 1270, 1330 and 1400 °C. The test was carried out in accordance to DIN EN 582 with a

velocity of 0.5 mm/min [28]. It is known from Dourandish et al. [29] that boron can increase tensile strength of composites, due to the formation of a Fe-B eutectic at 1170 °C, which enables an improved wetting of the ceramic material. To investigate this 0.03 and 0.63 wt% amorphous boron was added to the ceramic layer. The test was done with a 100 kN universal testing machine (Zwick GmbH, Germany) (figure 2). For this, the metallic layers were glued to the testing stamps with FM®1000 gluing pads (Cytec Industries Corp., USA).

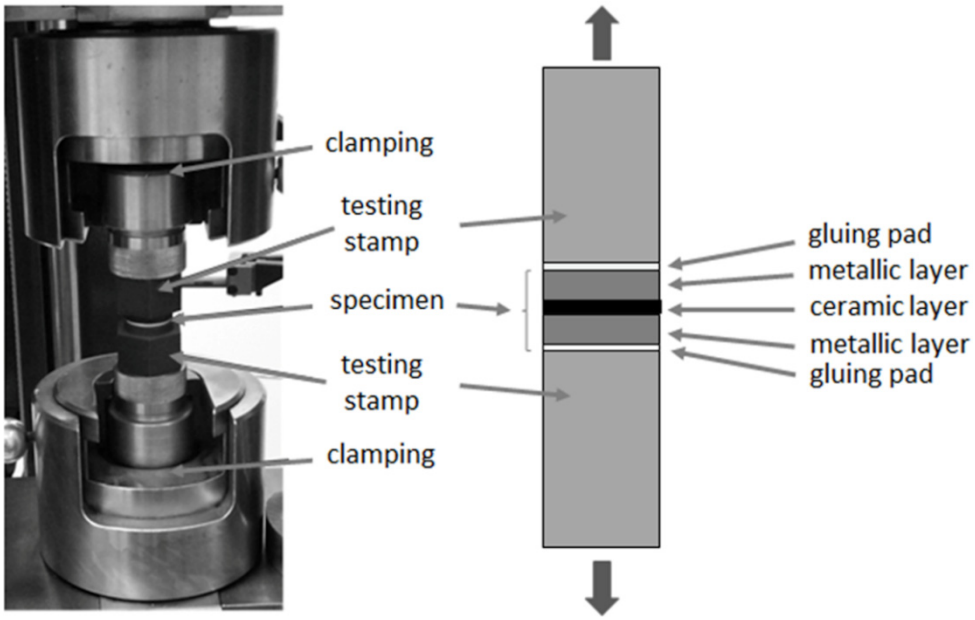

Figure 2. Universal testing machine (left) and scheme of the experimental build up for testing the adhesive tensile strength.

3. Results and Discussion

3.1. CTE and sintering behaviour

Figure 3 shows the CTE of the used materials up to a temperature of 1200 °C. CTEs match well to each other until 700 °C, with a maximum mismatch below 1.0×10^{-6} 1/K. With increasing temperature especially the CTE of the metallic material increases, which leads to a mismatch of 2.4×10^{-6} 1/K at 1200 °C [18]. However, it has to be assumed that the gap between the CTEs at higher temperatures isn't as bad as at lower temperatures because the metallic material has a low elasticity/viscosity at higher temperatures. Hence, the metallic layer can absorb some occurring stresses by deformation. Furthermore, other metallic materials and especially the austenitic steels 17-4PH or 316L, which are often used for the combination with zirconia, have much higher CTE's and with this, higher mismatches [30].

Figure 4 compares the sintering behaviour of ceramic and the four different metallic powders as a function of temperature and dwell time. The TZ-3YS-E powder starts sintering at 1150 °C. Its linear shrinkage at the end of the dwell time amounts 23.5%.

Metal powder 1 starts sintering in the same temperature region (1150 °C) as the TZ-3YS-E. Hereby, also the course of shrinkage exhibits a good agreement until the beginning of the dwell time.

This leads to a good accordance of the sintering strain rates (figure 5) and, furthermore, only a small maximum mismatch in strain rate of $\pm 0.25 \times 10^{-3}$ 1/min (figure 6) until the beginning of the dwell time. The mismatch in strain rate increases up to a maximum value of -0.75×10^{-3} 1/min due to the lower strain rate of metal powder 1 in the first 30 minutes of the dwell time.

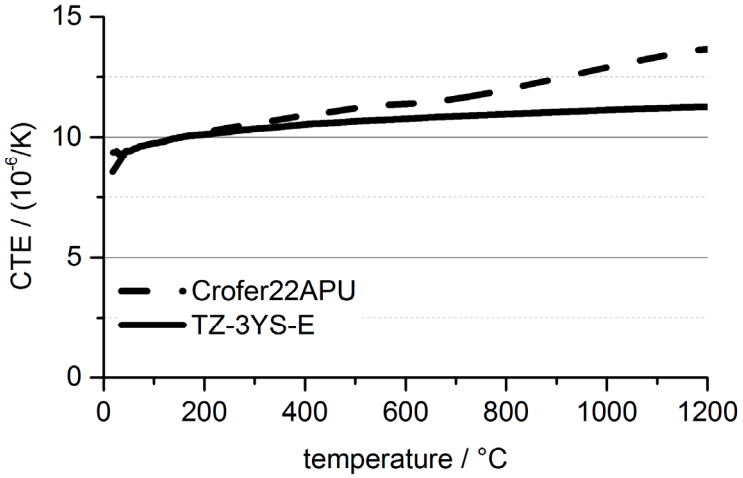

Figure 3. Coefficient of thermal expansion of the zirconia and the Crofer22APU.

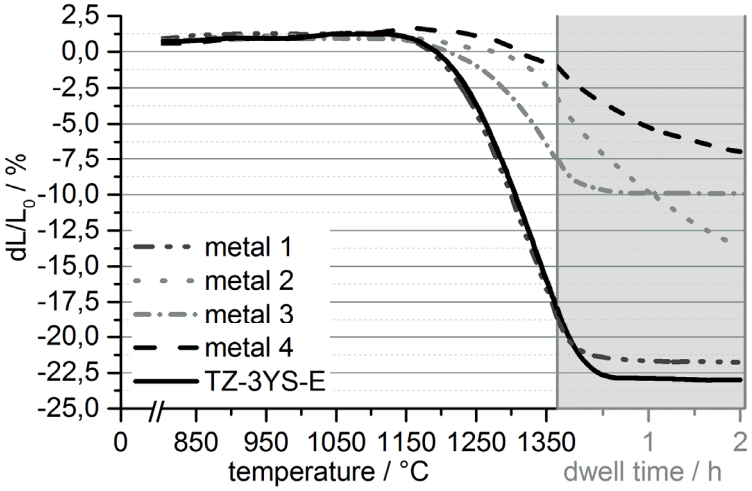

Figure 4. Sintering behaviour of the ceramic and metallic materials up to 1365 °C with a heating rate of 3 K/min and a dwell time of 2 h under argon (95%)/hydrogen (5%) atmosphere.

In comparison to powder 1, all other metallic powders start sintering at higher temperatures. Furthermore, their strain rates are significantly lower which results in lower total shrinkage values of 16.5% for powder 2, 10% for powder 3 and 7.5% for powder 4, respectively.

The later onset of sintering, as well as the lower maximum sintering strain rates, result in higher differences in strain rate. Composite 3 has a maximum mismatch at 1280 °C of -2×10^{-3} 1/min, while composite 2 and 4 have the highest mismatch values at -3×10^{-3} 1/min (figure 6).

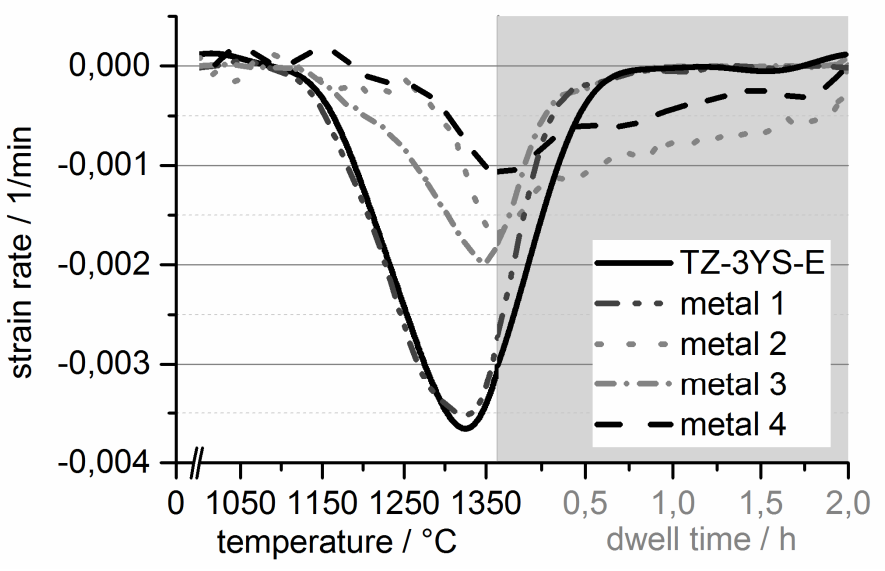

Figure 5. Sintering strain rate of the TZ-3YS-E and the 4 metallic powders up to 1365 °C with a heating rate of 3 K/min and a dwell time of 2 h under argon (95%)/hydrogen (5%) atmosphere.

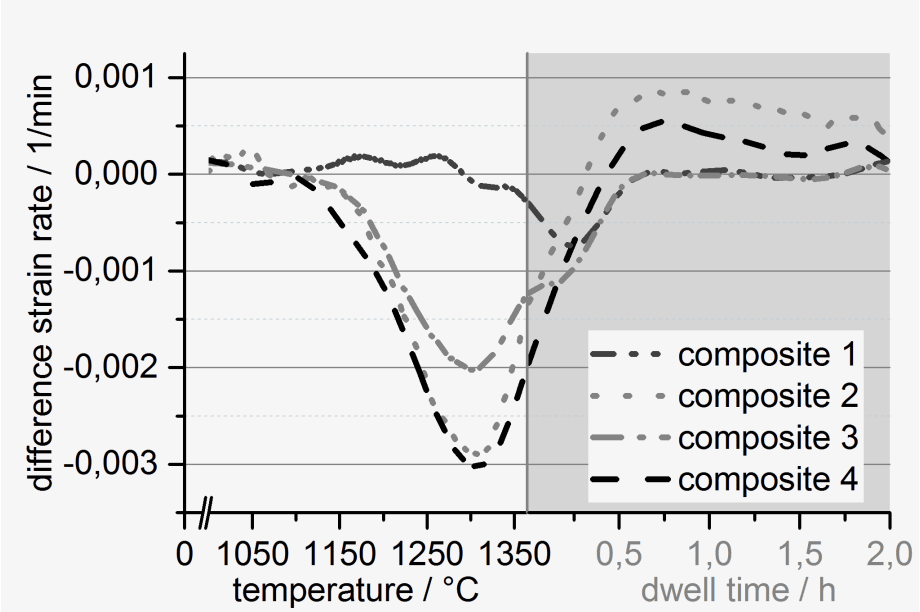

Figure 6. Differences in sintering strain rate of the 4 metallic powders minus TZ-3YS-E up to 1365 °C with a heating rate of 3 K/min and a dwell time of 2 h under argon (95%)/hydrogen (5%) atmosphere.

3.2. Sintering results

Figure 7 presents FESEM images of the microstructure of pure 1000 µm thick zirconia tapes after sintering for 2 h at 1350 and 1400 °C. Analysis exhibited that the porosity at 1350 °C amounts 4.2%, while increasing sintering temperature to 1400 °C decreases porosity below 1%.

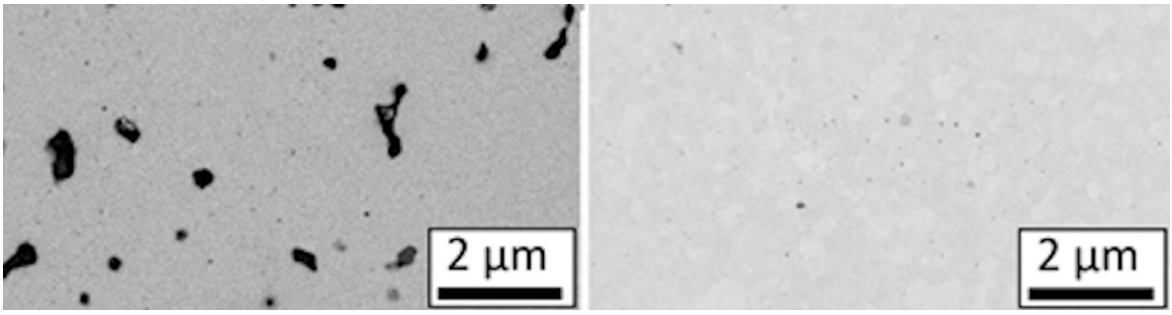

Figure 7. Electron scanning microscopy pictures of the ceramic microstructure sintered at 1350 °C and 1400 °C with a heating rate of 3 K/min and a dwell time of 2 h under argon (95%)/hydrogen (5%) atmosphere.

The asymmetric composites 1a and 2 were sintered with and without a coverage. While the mismatches in strain rate led to a warpage of the uncovered composites (figure 8), the coverage completely avoided a warpage. Thereby the coverage led to no macroscopic cracks on the surface of the composites. Considering figure 8, it is visible that the higher mismatch in strain rate of composite 2 in comparison to composite 1a led to a more significant warpage, despite its higher metallic layer thickness.

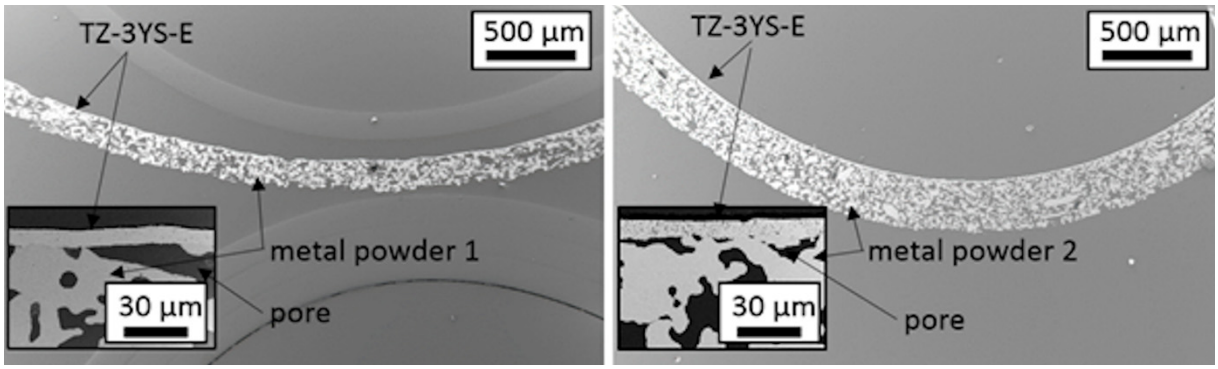

Figure 8. SEM images of asymmetric composites 1 (left) and 2 (right) after sintering for 2 h at 1350 °C without a coverage.

It is reducible to differences in viscosity that the much thinner ceramic layer (green thickness 11.6 µm) can bend the whole composite with a metallic layer thickness between 200 µm (composite 1a) and 400 µm (composite 2). Figure 9 shows the temperature- and density-dependent viscosity of the ceramic layer and metal powder 1 during sintering. The ceramic material starts with a viscosity of 1100 GPa*s at 1150 °C. At lower temperatures, the viscosity was too high so that no measurements were possible. With increasing sintering temperature, viscosity decreased to 20 GPa*s. During dwell time, further sintering and densification led to an increase of the viscosity up to 250 GPa*s. The same response exhibits the metallic material, whereby its viscosity is the whole time 1 to 2 magnitudes lower, which is the reason for that the thin ceramic layer can bend the whole composite. The measured viscosity values, thereby match well with already published values from literature (24, 25).

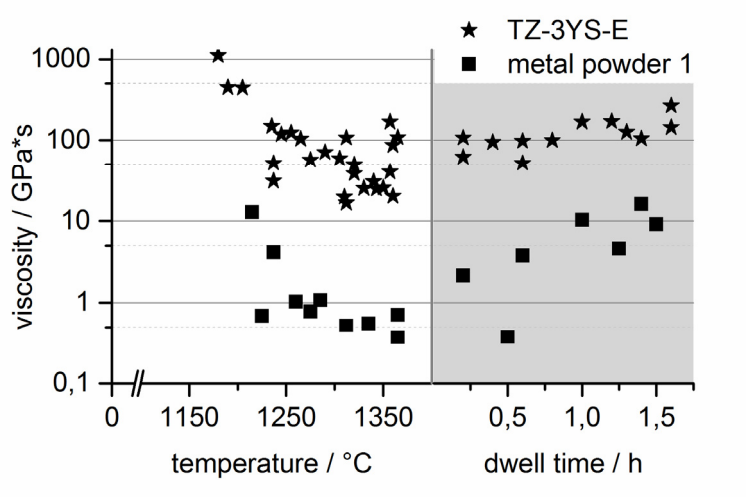

Figure 9. Viscosity of TZ-3YS-E and metal powder 1 during sintering.

Figure 10 shows the porosity of the free sintered ceramic layer (TZ-3YS-E) as well as the porosity of the co-sintered ceramic layers of composite 1a and 2 at different temperatures with a dwell time of 2 h, covered and uncovered. Comparing porosities of the uncovered composites at 1350 °C with the free sintered zirconia layer, it is obvious that the sintering behaviour of the zirconia layer is influenced by the metallic substrate. The porosity of composite 2 amounts 7.5%, which is 3% higher than the porosity of the free sintered zirconia layer, while the porosity of composite 1a is 1.5% lower than the porosity of the free sintered layer. This is caused by compression stresses (composite 1a) and tensile forces (composite 2), respectively, which improve respectively reduce sinter activity of the zirconia layer.

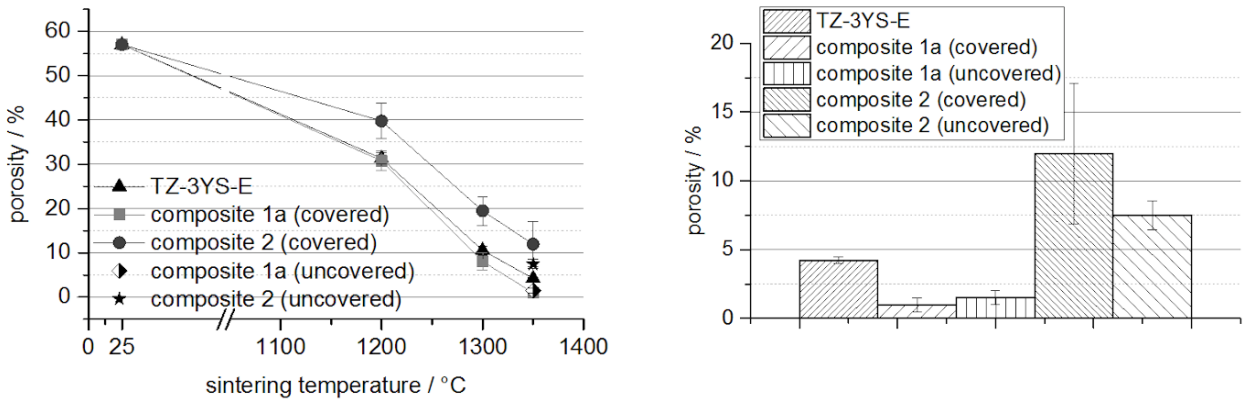

Figure 10. Porosity after sintering of a single zirconia tape (TZ-3YS-E) and the zirconia layer sintered as composite at different temperatures, a heating rate of 3 K/min and a dwell time of 2 h (left) and sintered at 1350 °C (right).

The negative influence is increased when the composite is covered during sintering. In this case, tensions cannot be prevented or relieved by a warping of the composite. Regarding the covered composite 2, it shows already at 1200 °C an 8% higher porosity than the free sintered layer. With increasing sintering temperature the mismatch is slightly increased up to 9%. Comparisons of the

covered and uncovered composites show that the porosity is 4% higher when it is covered during sintering. In contrast to these results, the coverage shows no negative influence in the case of composite 1. Here, both ceramic layers have porosities around 1%.

Further investigations, using symmetric structured composites out of the combination 1s, 3 and 4, confirm these results (figure 11). After sintering at 1350 °C, the porosity of the zirconia layer of composite 3 and 4 amount 11%, respectively 15%, while composite 1s has a porosity of 2%. The porosity of composite 4 is higher than the porosity of composite 3, due to its lower lateral shrinkage.

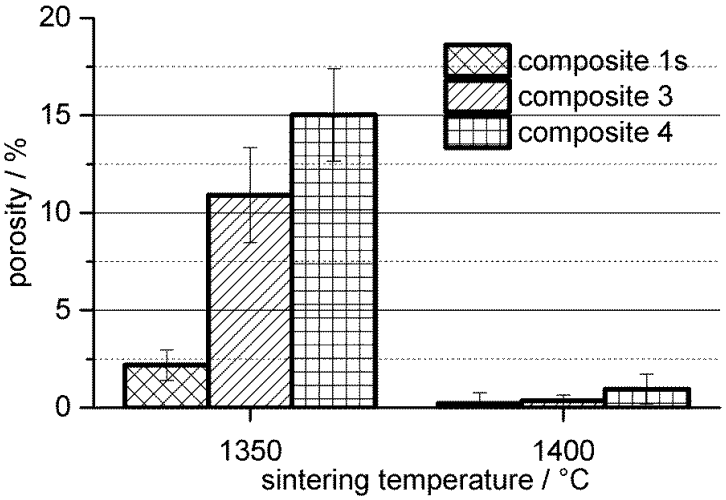

Figure 11. Porosity of zirconia layer of composite 1, 3 and 4 after sintering for 2 h at 1350 °C respectively 1400 °C with a heating rate of 3 K/min under argon (95%)/hydrogen (5%) atmosphere.

Nevertheless, an increase of the sintering temperature up to 1400 °C minimizes the negative effect of the metallic layers on densification of zirconia layers. At this temperature, the porosity is in all cases below 1%. This is also visible in the scanning microscopy images of the composites in figure 12 on the right hand side.

The lateral shrinkage of the ceramic layers in the case of composite 3 and 4 is constraint due to the metallic substrate. Accordingly, densification of the ceramic layer at 1400 °C is only possible with an increased shrinkage in thickness direction. This is evidenced by measurements of the thickness before and after sintering (table 2). In green state the ceramic layer thickness amounts in all cases 11.6 µm. At 1400 °C the ceramic layer thickness is between 9.5 and 8.2 µm, depending on the composite composition. Composite 1s has the biggest layer thickness after sintering, because the metallic substrate has nearly the same lateral shrinkage as the pure zirconia layer. This leads to a calculated shrinkage in thickness-direction of 18.1%. In the case of composite 3 and 4 the metallic layers have lower lateral shrinkage values, which leads to an increased shrinkage in z-direction of 27% and 29% respectively.

Table 2. Ceramic layer thickness of symmetric composites 1, 3 and 4 before and after co-sintering at 1400 °C.

composite	green	1400 °C	
	layer thickness/µm	layer thickness/µm	shrinkage/%
1	11.6 ± 1.0	9.5 ± 1.4	18.1
3		8.5 ± 1.4	26.7
4		8.2 ± 1.2	29.3

The results show that it is possible to densify the zirconia layer, even in combination with a high mismatch in strain rate. Despite these results, an adaptation of the sintering behaviour is indispensable. This is visible in the FESEM-images with lower magnifications (left hand side and middle in figure 12). While composite 1s has a completely defect free zirconia layer which is necessary for the different applications, sintering of both other composites is possible but they exhibit (micro-) cracks in the ceramic layer. Hence, a good adaption of sintering behaviour is necessary to achieve defect free composites.

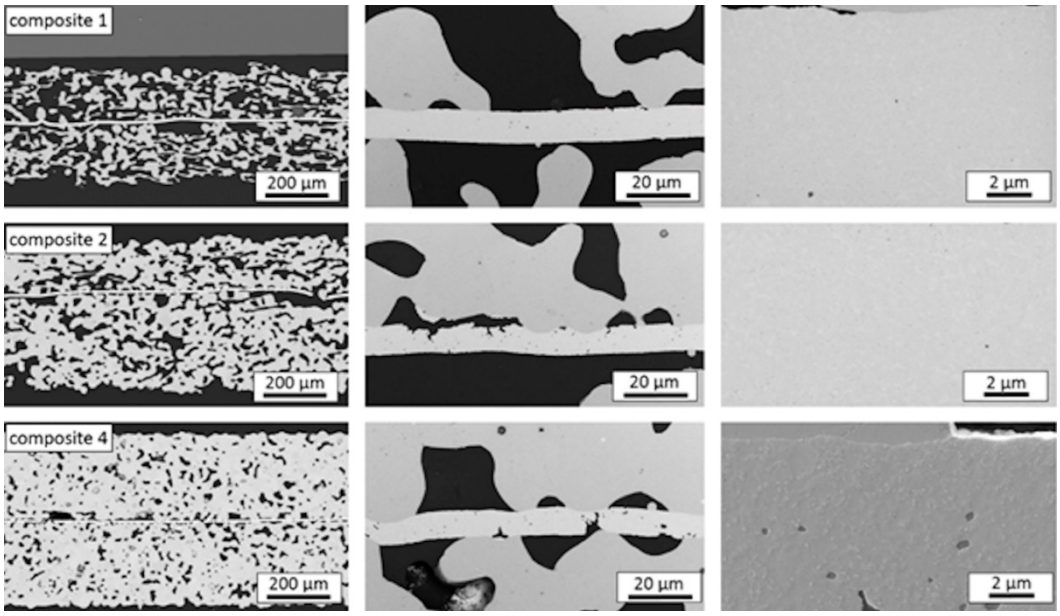

Figure 12. Scanning electron microscopy image of composite 1, 3 and 4 sintered for 2 h at 1400 °C, a heating rate of 3 K/min under Argo (95%)/Hydrogen (5%) atmosphere.

3.3. X-ray diffraction measurements

Figure 13 shows x-ray diffraction measurements of the zirconia layer of composite 1a before and after sintering. As the measurements show, before sintering the powder has some monoclinic phases which are non-existent after sintering. This result is independent of the investigated composite (composite 1a or 2) and demonstrates that a mismatch in CTE above 700 °C, does not lead to a stress induced transformation of the tetragonal in the monoclinic phase.

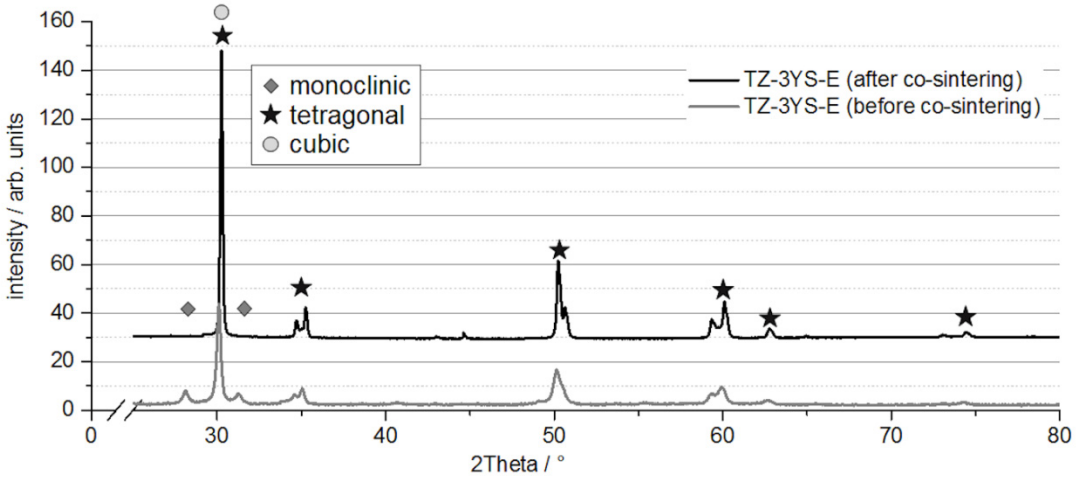

Figure 13. XRD-analysis of the zirconia layer of the asymmetric composite 1a after sintering at 1350 °C.

3.4. Interphase and adhesive tensile strength

The formation of mixed oxide phases [18] as well as a mechanical grouting is the bases of bonding between both materials.

Figure 14 left shows a metal-ceramic-metal composite consisting of a dense metallic layer (porosity < 3%) in combination with the zirconia layer. As the higher magnification at the right side of the figures shows, there is a 0.5 µm thick mixed oxide phase in the interface of both materials. The EDX measurement of this phase shows, that in addition to the main elements of both materials there exist an accumulation of different alloying elements as Al, La, Si. These elements can form phases as La_2O_3, $AlLaO_3$ or for example $ZrSiO_4$.

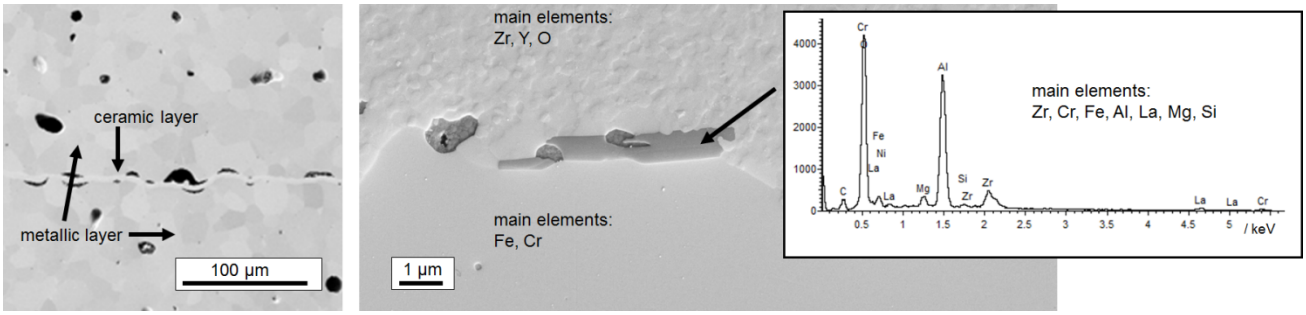

Figure 14. Scanning electron microscopy image of a metal-ceramic-metal compound with dense metallic layers (left) and the EDX-measurement of the interphase phase (right).

Measurements of the adhesive tensile strength of composite 1s (porous metallic layer) exhibit a high dependency on sintering temperature (figure 15). Starting with a tensile strength between 1 and 2 MPa at 1270 °C it is increased up to 4–5 MPa at 1330 °C. Thereby, also a slight increase of the strength with increased boron content is visible. An increase of the sintering temperature up to

1400 °C doubled tensile strength to 8 MPa without boron. Hereby, the strongest influence of the boron content is visible with an increase up to 9.6 MPa with 0.03% boron and up to 10.8 MPa with 0.63%. Regarding the use of boron, it has to be assumed that boron can lead to the formation of glass phases in the zirconia material which can negatively influence its properties. So, according to the specific application, the use of boron has to be reconsidered.

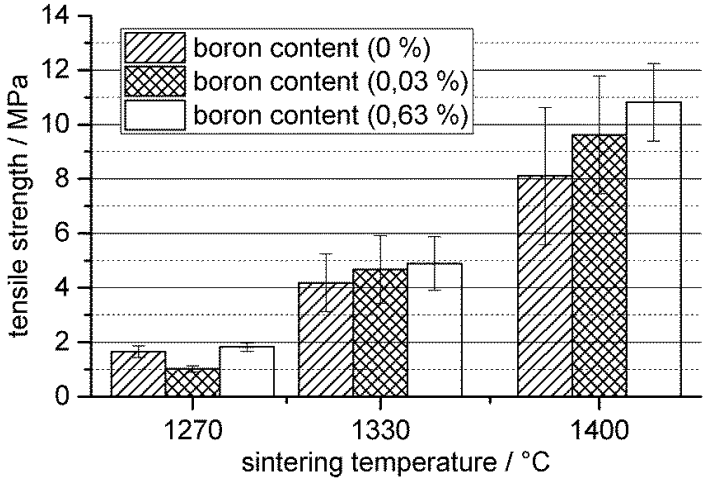

Figure 15. Tensile strength of the symmetric composite 1 in terms of sintering temperature and boron content.

The experiments exhibited that the composite breaks preferably at one metal ceramic interface, while the ceramic layer stays intact. This is visible in figure 16, which shows a top view on the ceramic layer after tensile tests. Some metallic particles are on top of the ceramic layer, which were pulled out of the metallic layer.

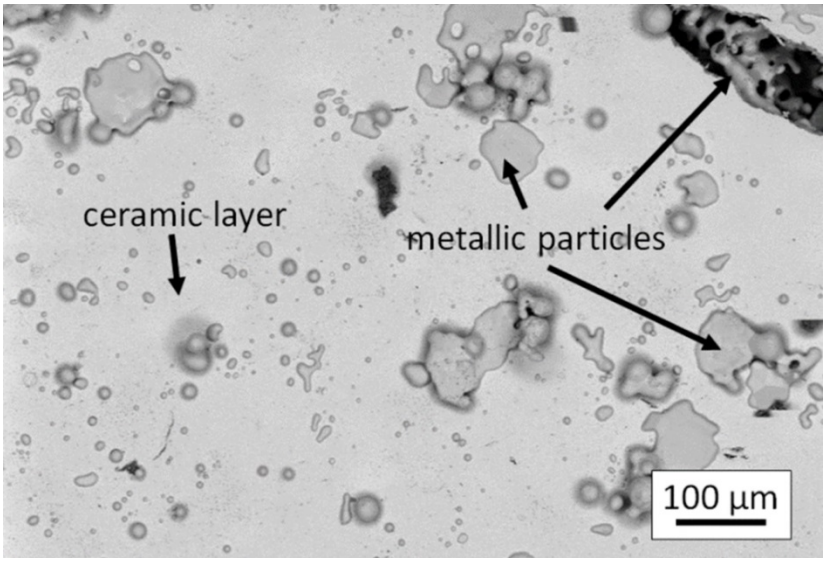

Figure 16. FESEM picture of the surface of ceramic layer of the symmetric composite 1 after tensile strength test.

Against the expectation tests of composites with dense metallic layers, sintered for 2 h at 1400 °C, showed, with a maximum tensile strength up to 3 MPa (without boron), much lower strengths. Measurements at lower sintering temperatures were not feasible, because they delaminated during clamping in the testing machine. Actually, a higher tensile strength was expected, due to the larger contact area between both materials.

A possible reason for this result can be assumed comparing the interface of the composites with dense metallic layers and porous metallic layers. Both show mixed oxide phase, while the only visible difference is, that the composites with the dense metallic layer have an interface with a lower roughness and less micro undercuts. Hence, the authors assume that especially the micro undercuts give strength and not the phases. So regarding design, undercuts or a materials gradient should be included in the composite. However, these results shall be proven in further investigations.

4. Conclusion

The presented work shows co-sintering results of metal-ceramic symmetric and asymmetric composites. The investigations exhibited that a mismatch in sintering behaviour due to a less shrinking metallic layer, led to a reduced density of the zirconia layer in comparison to a free sintered zirconia layer after sintering. Furthermore, mismatches in the strain rate cause cracks in the ceramic layer.

On the other hand, adapting of sintering behaviour allows manufacturing of defect-free metal-ceramic composites with dense ceramic layers. Largest dimensions of manufactured composites were 10 cm × 10 cm. X-ray diffraction measurements exhibited that there was no stress induced transformation from the tetragonal to the monoclinic phase due to mismatches in the CTE.

Adhesive tensile strength measurements showed a strong dependence of strength in terms of sintering temperature and boron content while maximum measured strength was 10.8 MPa.

Acknowledgement

This project was funded by the German Ministry of Economic Affairs and Energy (BMWi) through the German Federation of Industrial Research Associations (“Arbeitsgemeinschaft industrieller Forschungsvereinigung - AiF”) under the IGF-project number 18520 BR.

Conflict of Interest

The authors declare no conflicts of interest regarding this paper.

References

1. Rooney M, Roberts JC, Murray GM, et al. (2000) Advanced Materials: Challenges and Oppertunities. *John Hopkins APL Technical Digest* 21: 516–527.
2. Butterman WC, Gilette RG (1990) Markets for new materials. New materials society: Challenges and opportunities U. S. Department of the Interior. 2: 1–47.
3. Dixon DG (1995) Ceramic matrix composite-metal brazed joints. *J Mater Sci* 30: 1539–1544.

4. Berger L-M, Barbosa MM, Martin H-P, et al. (2013) Potential of Thermal Spray Technologies for the Manufacture of TEG. Thermoelectrics Goes Automative II (Thermoelectrics III), expert Verlag, Renningen, 260–272.
5. Cai PZ, Green DJ, Messing GL (1997) Constrained Densification of Alumina / Zirconia Hybrid Laminates, I: Experimental Observation of Processing Defects. *J Am Ceram Soc* 50: 1929–1939.
6. Chang J, Guillon O, Rödel J, et al. (2008) Characterization of warpage behaviour of Gd-doped ceria/NiO-yttria stabilized zirconia bi-layer samples for solid oxide fuel cell. *J Power Sources* 185: 759–764.
7. Ravi D, Green DJ (2006) Sintering stresses and distortion produced by density differences in bi-layer structures. *J Eur Ceram Soc* 26: 17–25.
8. Reynier T, Bouvard D, Carry CP, et al. (2012) Co-sintering of an anode-supported SOFC based on scandia stabilized zirconia electrolyte. *Advances in Science and Technology II: Ceramic Transaction* 232: 91–99.
9. Guillon O, Krauß S, Rödel J (2007) Influence of thickness on the constrained sintering of alumina films. *J Eur Ceram Soc* 27: 2623–2627.
10. Kim J-S, Rudkin RA, Wang X, et al. (2011) Constrained sintering kinetics of 3YSZ films. *J Eur Ceram Soc* 31: 2231–2239.
11. Muecke R, Menzler NH, Buchkremer H-P, et al. (2009) Cofiring of Thin Zirconia Films during SOFC Manufacturing. *J Am Ceram Soc* 92: 95–102.
12. Yamaguchi T, Suzuki T, Shimizu S, et al. (2007) Examination of wet coating and co-sintering technologies for micro-SOFCs fabrication. *J Membrane Sci* 300: 45–50.
13. Baumann A (2010) Powder injection moulding of metal-ceramic composites, PhD-thesis, Berg-akademie Freiberg.
14. Yeo J-G, Jung Y-G, Choi S-C (1998) Zirconia-stainless steel fuctionally graded material by tape casting. *J Eur Ceram Soc* 18: 1281–1285.
15. Hage C (2013) Fundamental aspects of 2 component powder injection moulding, PhD-thesis, Karlsruher Institute of Technology.
16. Shen Z, Zhu X, Le S, et al. (2012) Co-sintering anode and Y_2O_3 stabilized ZrO_2 thin electrolyte film for solid oxide fuel cell fabricated by co-tape casting. *Int J Hydrogen Energ* 37: 10337–10345.
17. Wu K, Scheler S, Park H-S, et al. (2013) Pressureless sintering of ZrO_2-$ZrSiO_4$/NiCr functionally graded materials with a shrinkage matching process. *J Eur Ceram Soc* 33: 1111–1121.
18. Slawik T, Bergner A, Puschmann R, et al. (2014) Metal-Ceramic Layered and Composites Manufactured Using Powder Techniques. *Adv Eng Mater* 16: 1293–1302.
19. Slawik T, Bergner A, Scheithauer U, et al. (2015) Adapting the co-sintering bahavior of metal-ceramic composites. Proceedings EuroPM2015.
20. Mistler RE, Twiname ER (2000) *Tape Casting–Theory and Practice.* Wiley-American Ceramic Society. 1 edition.
21. Scheithauer U, Slawik T, Schwarzer E, et al. (2015) Manufacturing of Metal-Ceramic-Composites by Thermoplastic 3D-Printing (3DTP). *J Ceram Sci Techn* 29: 125–132.
22. Slawik T, Moritz T, Scholl R, et al. (2013) Multilayered metal-ceramic composites made by coating technologies Proceedings 8. Pacific Rim International Conference on Advanced Materials and Processing.

23. Bergner A (2014) Steel-ceramic laminates made by tape casting - Processing and Interfaces. Singh JP, Bansal NP, Bhalla AS, et al. (Editors). *Processing and Properties of Advanced Ceramics and Composites VI* 249: 53–63.
24. Hagy HE (1963) Experimental Evaluation of Beam-Bending Method of Determining Glass Viscosities in the Range 10 8to 10 15 Poises. *J Am Ceram Soc* 46: 93–97
25. Lee S-H, Messing GL, Green DJ (2003) Bending Creep Test to Measure the Viscosity of Porous Materials during Sintering. *J Am Ceram Soc* 86: 877–882.
26. Lame O, Bouvard D, Wiedmann H (2002) Anisotropic shrinkage and gravity induced creep during sintering of steel powder compacts. *Powder Metall* 45: 181–185.
27. Blaine DC, Bollina R, Park S-J, et al. (2005) Critical use of video-imaging to rationalize computer sintering simulation models. *Comput Ind* 56: 867–875.
28. Jankowski AF (1987) Adhesion of physically vapor-dposited titanium coatins to beryllium substrates. *Thin Solid Films* 154: 183–198.
29. Dourandish M, Simchi A, Shabestary ET, et al. (2008) Pressureless Sintering of 3Y-TZP/Stainless-Steel Composite Layers. *J Am Ceram Soc* 91: 3493–3503.
30. Dourandish M, Simchi A (2009) Study the sintering behaviour of nano-crystalline 3Y-TZP/430L stainless-steel composite layers for co-powder injection molding. *J Mater Sci* 44: 1264–1274.

AIMS Press